J. Fluid Mech. (2007), *vol.* 574, *pp.* 343–364.
doi:10.1017/S0022112006004125 Printed in the United Kingdom

Forced dewetting on porous media

OLIVIER DEVAUCHELLE, CHRISTOPHE JOSSERAND AND STEPHANE ZALESKI

Laboratoire de Modélisation en Mécanique, CNRS-UMR 7606, Case 162, 4 place Jussieu, 75252 Paris Cédex 05, France

(Received 26 July 2005 and in revised form 5 September 2006)

We study the dewetting of a porous plate withdrawn from a liquid bath. The contact angle is fixed to zero and the flow is assumed to be almost parallel to the plate (lubrication approximation). The ordinary differential equation involving the position of the water surface is analysed in phase space by means of numerical integration. We show the existence of a stationary moving contact line with zero contact angle below a critical value of the capillary number $\eta U/\gamma$. Above this value, no stationary contact line can exist. An analytical model, based on asymptotic matching is developed, which reproduces the dependence of the critical capillary number on the angle of the plate with respect to the horizontal (3/2 power law), provided the capillary length is much larger than the square root of the porous-medium permeability. In addition, it is shown that the classical lubrication equation leads not only to the well-known Landau–Levich–Derjaguin films, but also to a family of films for which thickness is not imposed by the problem parameters.

1. Introduction

When sea retreats from the shore, sand structures appear as solid granular particles are transported *via* the liquid. Liquid motion and particularly film retraction on an erodible medium are known to create impressive erosion patterns, such as sand ripples for oscillatory waves (Scherer, Melo & Marder 1999; Stegner & Wesfreid 1999) or sand furrows (Daerr *et al.* 2003; Schorghofer *et al.* 2004). The case of liquid retraction from a granular bed can be understood as a dewetting dynamics on a porous erodible bed. Such physical phenomena have been reproduced in the laboratory by pulling a plate covered with a bed of grains out of a liquid bath (Daerr *et al.* 2003). This is similar to the well-known experiment investigating a moving contact line on a non-porous plate (Blake & Ruschak 1979). In this latter case, a contact line exists for small removal speed U, whereas for higher speed (above a well-defined critical value U_{cr}) a macroscopic water film (the so-called Landau–Levich–Derjaguin (LLD) film, see Landau & Levich 1942; Derjagin 1943) covers the whole plane (Eggers 2004*a*). We propose here to investigate this transition for a saturated porous medium, in connection with recent experiments involving granular materials by Daerr *et al.* (2003). There, a motor-driven plane, covered with a granular layer, is withdrawn from a water tank at constant speed U. The solid plane is tilted to an angle θ. At high enough velocity, erosion river networks and mudflows are observed, whereas only light patterns appear at smaller speed. We investigate the loss of a static contact line and seek to relate it to the transition between various erosion regimes. We therefore seek the critical velocity above which no static contact line can exist on a granular bed. Below this critical velocity, almost no grain motion is observed so that we identify

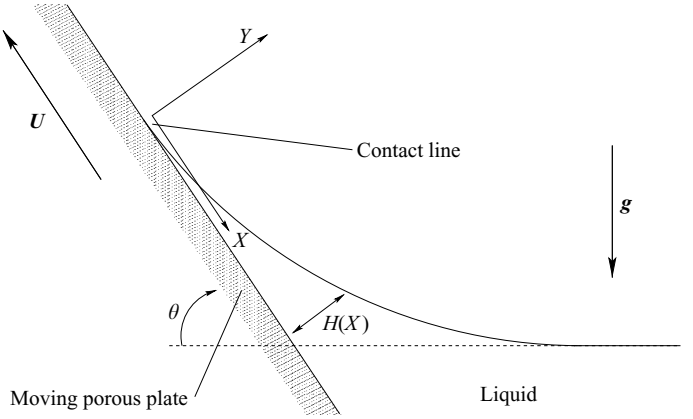

FIGURE 1. A porous plate of conductivity k is being withdrawn from a liquid bath with speed $\boldsymbol{U}$ at angle θ. h, x and y are the non-dimensional counterparts of H, X and Y.

the granular bed with a rigid porous medium. Dewetting on a porous medium has already been studied in different configurations (see Raphaël & de Gennes 1999; Aradian, Raphaël & de Gennes 2000; Bacri & Brochard-Wyart 2001 and references therein). The case of a porous plate removed from a liquid was studied by Raphaël & de Gennes (1999), but the focus was on the spatial evolution of the LLD film, the existence of which was assumed. The contact-line dynamics was also studied (Aradian *et al.* 2000) on a horizontal porous plate into which a liquid film is sucked. From a more theoretical point of view, the problem of a moving contact line on a porous solid is pointed out by de Gennes (1985) as a natural regularization for the contact-line dynamics equations. The bulk liquid flow through the porous solid indeed removes the usual stress singularity that would be encountered at a contact line with a no-slip condition (Dussan V. & Davis 1974). No additional assumption, such as the introduction of a Navier slip at microscopic scale, is then required. However, another question arises when considering a porous medium: what is the relevant condition for the contact angle at the contact line? As discussed below, we propose here for a saturated system to take a zero contact angle.

The paper is organized as follows. In § 2, we use the lubrication approximation to deduce the equation for the static interface shape, both for the contact line and a film solution that does not remove or add water to the tank, hereinafter referred to as a *zero-flux film* (a true LLD film has a finite flux, and its equation is different, see Appendix A). In § 3, we exhibit numerically the transition between these two configurations as the pulling velocity increases. Then, we propose to interpret the solutions in the framework of dynamical systems (§ 4).

2. Principles

2.1. *Lubrication approximation*

Our approach seeks to determine the velocity (if any) above which the static contact line can no longer exist in a granular bed withdrawal experiment. Below this velocity, we can consider that the grains barely move with respect to the withdrawn plate. Thus, the granular material is represented by a non-erodible porous medium (see figure 1) of permeability k, and we only have to investigate the stationary problem. The fluid is characterized by its density ρ, viscosity η and surface tension γ. Assuming invariance

in the Z-direction, we consider the two-dimensional problem where the water surface is described by the function $H(X)$. At the beginning of the experiment, the porous plate is saturated with water. For the plate velocities pertinent to the problem (typically $0.5\,\mathrm{cm\,s^{-1}}$) and the estimated porosity of the granular bed ($k \approx 10^{-12}\,\mathrm{m^2}$), we can consider that the porous medium remains fully saturated with water at any distance from the free water level.

We will restrict our analysis to small angles θ so that the lubrication approximation can be employed (i.e. $(\theta, \|H'\|) \ll 1$ where the prime stands for the X-derivative). Only the X-component u of the velocity has to be taken into account, for which Poiseuille profile is assumed, with a vanishing tangential stress on the gas side:

$$\left.\frac{\partial u}{\partial Y}\right|_{Y=H(X)} = 0. \tag{2.1}$$

Another boundary condition has to be written at the porous surface. The classical no-slip condition, as required at the solid-fluid interface on an impermeable plate, leads to the following equation for $H(X)$ (its derivation is similar to that presented in Appendix A):

$$H''' + \frac{1}{l_c^2}(-H' + \theta) = \frac{3Ca}{h^2}, \tag{2.2}$$

where l_c and Ca are, respectively, the capillary length ($l_c \approx 2.8\,\mathrm{mm}$ for water) and the capillary number, defined by

$$Ca = \frac{\eta U}{\gamma}, \qquad l_c = \sqrt{\gamma/\rho g}.$$

Equation (2.2) and any derivative of its solutions are singular at the contact line, where $H = 0$ (Duffy & Wilson 1997). For a non-porous surface, a short-length regularization is invoked coming either from effective slip near the contact line (Huh & Scriven 1971), the existence of a pre-wetting liquid film and van der Waals forces (de Gennes 1984; Hervet & de Gennes 1984) or a 'diffuse interface model' (Seppecher 1996). Such a regularization always involves a microscopic cutoff length (of the order of 1 nm) below which it is claimed that hydrodynamics fails. The Navier slip condition is then mostly used in numerical simulations investigating moving contact line problems (Renardy, Renardy & Li 2001). At the solid–fluid interface: $u - U = \lambda_N \partial u/\partial Y$ at $Y = 0$ where λ_N is the cutoff length. With this boundary condition, (2.2) becomes

$$H''' + \frac{1}{l_c^2}(-H' + \theta) = \frac{Ca}{H^2/3 + \lambda_N H}. \tag{2.3}$$

Equation (2.3) can be numerically solved and analytically approached. A contact line is then found to exist as long as the capillary number is smaller than a critical value, above which a macroscopic LLD film is deposited on the solid (Eggers 2004*a*). However, not all the singularities discussed above are suppressed by the Navier slip condition since the capillary pressure still diverges at the contact line (see Appendix B).

2.2. *The case of a porous solid*

A porous solid allows for both interfacial slip (first proposed by Beavers & Joseph 1967) and bulk flow. Using the Brinkman equation to describe the flow inside the porous medium, Neale & Nader (1974) showed that, for a homogeneous porous

medium, the magnitude of the slip is proportional to the prevailing shear stress:

$$u|_{Y=0} - u_p|_{Y=0} = \frac{\sqrt{k}}{\alpha} \left. \frac{\partial u}{\partial Y} \right|_{Y=0}, \tag{2.4}$$

where k is the permeability of the solid, and u_p the velocity of the fluid in the porous medium (note that this relation holds both in the laboratory frame and in the porous plate). α is a coefficient of order one which must be experimentally measured. It has been identified by Neale & Nader (1974) to $\sqrt{\mu^*/\mu}$ where μ^* is the effective dynamical viscosity of the fluid in the porous medium, used in the Brinkman equation. α was experimentally measured for different porous media and different fluids, and was found to vary generally between 0.1 and 4. The Brinkman equation produces a boundary layer (of typical depth $\sqrt{k}$) in the porous medium (Goyeau *et al.* 2003), below which the flow follows Darcy's law.

Now, if the porous plate is thin enough (see Appendix C), the water flow inside the porous medium is nearly one-dimensional, and is controlled by the pressure boundary condition at the interface with free water. Finally, let us assume that the plate remains fully saturated during the entire experiment, which is true for a sufficient withdrawal velocity. Darcy's law is

$$u_p + U = -\frac{k}{\eta}\left(\frac{\partial p_p}{\partial X} - \rho g \theta\right), \tag{2.5}$$

(where p_p is the water pressure in the porous medium) and finally the following equation describes the shape of the steady fluid film under withdrawal (the detailed derivation is presented in Appendix A):

$$H''' + \frac{1}{l_c^2}(-H' + \theta) = \frac{Ca}{H^2/3 + \sqrt{k}H/\alpha + k}.$$

If we choose l_c as a length scale for both H and X (i.e. $H = l_c h$ and $X = l_c x$), the above equation becomes

$$h''' - h' + \theta = \frac{Ca}{h^2/3 + \lambda h/\alpha + \lambda^2}. \tag{2.6}$$

where $\lambda = \sqrt{k}/l_c$. h and x are now non-dimensional quantities (and will remain so hereinafter). Such an equation is similar to those studied for the contact line on a solid surface, using specific boundary conditions at the solid surface (Hocking 2001; Eggers 2004*a*). It has been shown (in the case of a plate pushed into water) that the details of the regularization do not influence the far-field fluid flow as long as the cutoff length is small enough (Eggers 2004*b*). However, an important difference in our case lies in the typical values of λ involved in porous media ($\approx 10^{-2}$ in Daerr *et al.* 2003) to be compared with 10^{-6} for regular solids.

Hadjiconstantinou (2003) and Maurer *et al.* (2003) use a second-order slip law to model the flow of gases at large Knudsen numbers. This boundary condition (adapted to the present notations) reads

$$u|_{Y=0} + U = \Lambda_C \left. \frac{\partial u}{\partial Y} \right|_{Y=0} - \alpha_C \Lambda_C^2 \left. \frac{\partial^2 u}{\partial Y^2} \right|_{Y=0},$$

where α_C is a positive coefficient of order one, and Λ_C is a slip length of the same order as the mean free path of the gas. If such a boundary condition were used at the solid–fluid interface in the case of a contact line, again equation (2.6) would be obtained.

2.3. *Boundary conditions*

The limit for large positive values of x is well-defined: the water surface is horizontal far from the plane, that is

$$h(x) \underset{x\to\infty}{\sim} \theta x. \tag{2.7}$$

For the two remaining boundary conditions, two different cases will be studied, depending on whether a contact line is formed between the water surface and the solid plate, or if a film of water remains on the solid surface. In the first case, the water level vanishes at the origin and a contact angle θ_0 is usually imposed; the *contact-line set* of boundary conditions is

$$h(0) = 0, \quad h'(0) = \theta_0. \tag{2.8}$$

In the present problem, three different contact angles may be defined, depending on the considered scale. At a scale smaller than the pore size, the *microscopic contact angle* is a chemical property fixed once the liquid, the gas and the solid are specified. This microscopic contact angle may be different from zero in this study. At a scale larger than the pore size, but smaller than the capillary length, one may define θ_0, which will hereinafter be referred to as the *contact angle* (θ_0). This angle results from pore-scales effects, and is analogous to the contact angle defined on an heterogeneous medium (see de Gennes, Brochard-Wyart & Quéré 2005). It may be affected by hysteresis, but in the present case, only its receding value need be considered. Finally, at the capillary length scale, an *apparent contact angle* (θ^*_{ap}) is defined mathematically as the limit of the meniscus solution slope when x tends to zero (see § 2.5 and Eggers 2004*a*).

To perform the present analysis, the contact angle θ_0 must be specified. The equations presented above rely on the assumption that the pore-scale effects, which are probably intermittent and heterogeneous for a receding contact line, may be represented by a mean value (namely θ_0) at larger scales. Following Raphaël & de Gennes (1999), we will hereinafter consider that the contact angle θ_0 is zero for dewetting on a porous medium. Although we did not find any proof for it, this assumption may be understood as follows: if the porous medium remains fully saturated, its surface (around $y = 0$) is rough and covered with water. If it is so, the microscopic contact angle is alternatively positive and negative (depending on which side of a bump the contact line is), and we consider here as a first approximation that its mean value is zero.

When an infinite film is drawn from the meniscus, the only boundary for the $x \to \infty$ condition known *a priori* is

$$\lim_{x\to-\infty} h(x) = h_f, \tag{2.9}$$

where h_f is a constant solution of (2.6). Note that (2.6) stands only for zero-flux films, that neither add nor withdraw water from the tank. The general case is presented is Appendix D. We omit the important case where an LLD film is continuously elongating with time, a case that was investigated by Hocking (2001). Our study is therefore relevant for determining the loss of a static contact line solution, without any information about the dynamics. The stability of the solution as well as the time-dependent dynamics of a moving meniscus cannot be studied at this stage and will be the purpose of further work. However, we will see in § 4 that the film solutions of (2.6) satisfying (2.9) play an important role in the dynamical system describing our solutions. Finally, for a solution to be acceptable, the water level must always lie above the porous medium: $\forall x, h(x) > 0$.

2.4. *Parameters*

The parameter α comes from the detailed modelling of the interface slip flow (see § 2.2). Its value, as long as it is positive and of order one, has a very small influence on the results presented here. Different values have been tested numerically, and the general patterns of the results (the contact-line transition in particular) remained unchanged. Mathematically, α does not change the asymptotic behaviour of the equation for both limit $h \to \infty$ and $h \to 0$, thus it can only affect the local behaviour of the solution when h is of order λ.

For the sake of simplicity, the coefficient α is fixed to one in the following, except in § 5 where it will be fixed to $\sqrt{3}/2$ to allow for analytical computation. The numerical computations are performed with $\alpha = 1$, and the comparison with analytical results still holds, providing support to the idea that the wetting transition is almost independent of α.

Now, for $\alpha = 1$, (2.6) is an ordinary differential equation (ODE) with three parameters: θ, Ca and λ. In fact, this equation is only a two-parameter ODE: defining $h_* = h/\lambda$, equation (2.6) becomes

$$h_*''' - h_*' + \theta^* = \frac{Ca^*}{h_*^2/3 + h_* + 1}, \tag{2.10}$$

where θ^* and Ca^* are defined as follows:

$$\theta^* = \theta/\lambda = \theta\sqrt{\frac{\gamma}{\rho g k}},$$

$$Ca^* = Ca/\lambda^3 = \frac{U\eta\sqrt{\gamma}}{(\rho g k)^{3/2}}.$$

Equation (2.10) is the one we will study later on, but we will omit the $_*$ on h_* for the sake of readability. These non-dimensional parameters were chosen because they are proportional to the two experimental parameters that may be easily and continuously tuned, namely U and θ. If the permeability of the porous solid is extremely low, both θ^* and Ca^* tend to infinity, as well as the ratio $Ca^*/\theta^* = U\eta/(\theta\rho g k)$. In this case, the velocity inside the porous medium is extremely slow compared to U. For the experimental study of Daerr *et al.* (2003), the rescaled capillary number Ca^* is of the order of 10^5.

2.5. *Hydrostatic solutions*

Any solution which respects the boundary condition (2.7) for large x satisfies

$$\lim_{x \to +\infty} h(x) = +\infty,$$

thus for large x, equation (2.10) becomes

$$h''' - h' + \theta^* = 0. \tag{2.11}$$

The behaviour of the water surface at large x, hereinafter denoted by h_∞, is directly obtained from (2.11):

$$h_\infty(x) = A_\infty + \theta^* x + (\theta^* - \theta_{ap}^*)\exp(-x), \tag{2.12}$$

where A_∞ and θ_{ap}^* are two constants, corresponding, respectively, to the length of the dynamical meniscus and to the so-called *apparent contact angle* (note that the dimensional apparent contact angle is actually $\theta_{ap}^*\lambda$). Thus, (2.11) leads to the classical static meniscus solution (remember that x has been scaled by the capillary length l_c).

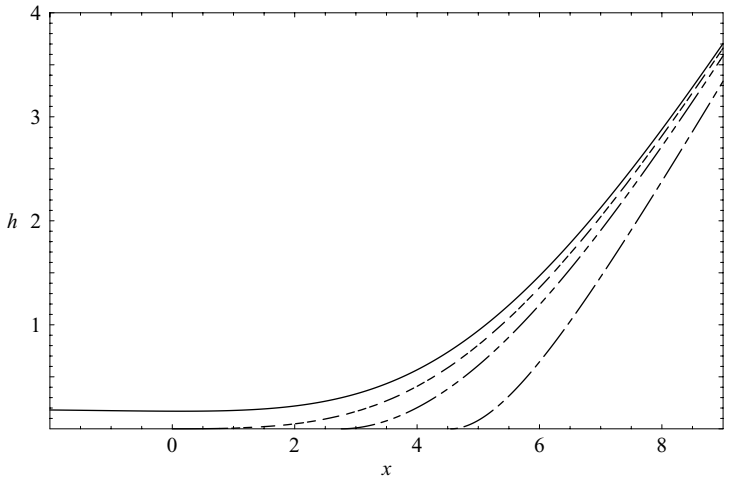

FIGURE 2. Numerical solutions of equation (2.10) for different capillary numbers, from bottom to top $Ca^* = 0.1$, 0.8, 1.0245, 1.2. The rescaled tilt angle θ^* is fixed to 1.

We may consider that (2.10) holds at any position on the x-axis, even though the flow may no longer be laminar far from the plate.

3. Numerical results

3.1. *Contact line solutions*

To seek steady contact line solutions, (2.10) may be solved numerically using a finite-difference algorithm. In the case of a contact line, two boundary conditions may be fixed at $x = 0$ by the contact-line conditions (2.8). The third condition comes from the flat water level at infinity (2.7) and we end up with the following system:

$$h''' - h' = f(h), \quad h(0) = h'(0) = 0, \quad h(x) \underset{x\to\infty}{\sim} \theta^* x, \tag{3.1}$$

where

$$f(h) = \frac{Ca^*}{h^2/3 + h + 1} - \theta^*.$$

We use a shooting method (see Manneville 1990), varying the initial curvature $h''(0)$ in order to find the numerical solution which corresponds to the hydrostatic condition at large x. Some numerical contact-line solutions to (3.1) are presented on figure 2 for different Ca^* at fixed θ^*. It is remarkable that contact-line solutions exist for non-zero capillary number and zero contact angle. Indeed, Eggers (2004*a*) showed that for a completely wettable plate ($\theta_0 = 0$), no contact line can exist for positive capillary number. The impregnation law used here as a boundary condition at the porous plate surface allows for such a counter-intuitive behaviour.

As shown in figure 2, the contact-line zone is somehow stretched as the capillary number is increased. In other words, the curvature $h''(0)$ at the origin tends to zero as Ca^* tends to a critical value Ca_c^*. Above this critical value, no contact-line solution can be found by the shooting method. This transition will be clarified below using the dynamical system associated to (3.1). The disappearance of the contact-line solution may be represented in a kind of bifurcation diagram, plotting the curvature at the origin against the capillary number, as shown in figure 3. Notice that, even though the

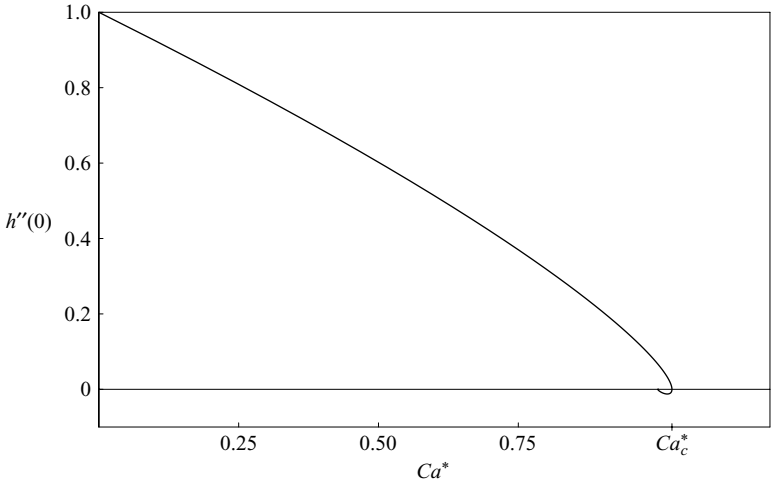

FIGURE 3. Curvature at the origin versus rescaled capillary number, for a contact-line solution of equation (2.10). The rescaled tilt angle θ^* is fixed to 1. No solution is found for capillary numbers higher than $Ca_c^* \approx 1.0247$.

curvature at the origin tends to zero as Ca_c^* is approached, the contact-line solution does not become unrealistic for $Ca > Ca_c^*$ owing to a negative initial curvature, but rather disappears through a bifurcation. Above the critical capillary number, no matching exists between the behaviour of the solution at the contact line and the gravity–capillary solution.

3.2. *Film solutions*

A zero-flux film solution can exist whenever there is a positive value h_f such that $f(h_f) = 0$, which occurs as soon as $Ca^* \geqslant \theta^*$. Two major limitations have to be pointed out for these film solutions: first, we might not be able to match this film solution to the hydrostatic region with h remaining positive everywhere. Moreover, we restrict our analysis here to an already established film of zero mass flux, whereas transitory (Hocking 2001) and finite flux solutions should be considered. In fact, the flux of the classical LLD film which covers a solid plate at sufficient velocity does not vanish (Landau & Levich 1942; Wilson 1982), the mathematical differences between LLD films and zero-flux films are presented in Appendix D. However, the focus here is on the disappearance of the contact-line solution, and in the following, we will restrict ourselves to the zero-flux equation. A complete study of the wetting transition should include the determination of the flux for the film solution. Numerically, above the critical capillary number Ca_c^*, we have always been able to find a zero-flux film of thickness h_f in the limit $x \to -\infty$ that could match to the hydrostatic solution without crossing $h = 0$ (see figure 2). Such a solution may be numerically approached, using a special shooting method described in § 4.1.1. We observed that as the capillary number is decreased, the film surface is shifted down along the y-axis (see figure 4), and we may define a second critical capillary number $Ca_{c,2}^*$, below which the film solution becomes negative in some region. Consequently, if $Ca_{c,2}^*$ is smaller than Ca_c^*, hysteresis may occurs, that is, two solutions, a contact-line one and zero-flux film one, may coexist for same tilt angle and capillary number.

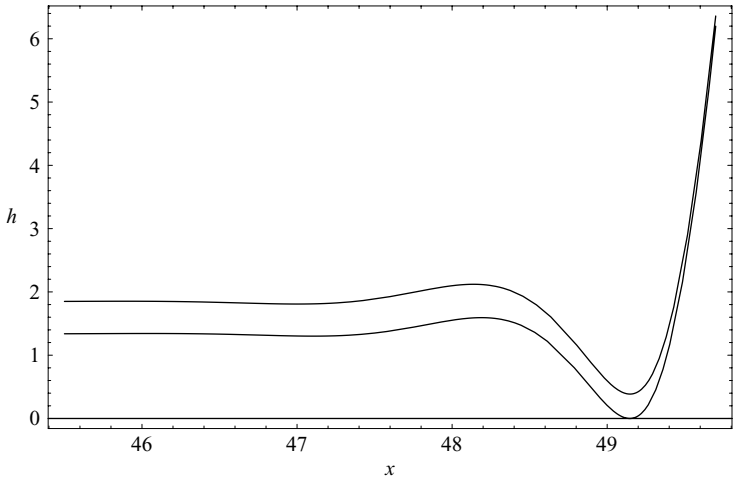

FIGURE 4. Two zero-flux film solutions for $\theta^* \approx 66.62$ at $Ca^* \approx 241.3$ (upper) and $Ca^* \approx 195.5$ (lower). The curve below corresponds to point A of figure 7: $h(x_{\min}) \approx 0$.

4. Dynamical systems interpretation

4.1. *Phase space*

In what follows, we interpret and develop the preceding results using dynamical system theory (Strogatz 1994). Let us consider the phase space $\mathscr{V}$ corresponding to (2.10), that is, $\mathbb{R}^3$ with coordinates (h, h', h''). Any solution of (2.10) is a trajectory of $\mathscr{V}$, parameterized by x, which satisfies

$$\boldsymbol{X}' = \boldsymbol{F}(\boldsymbol{X}) = \begin{pmatrix} h' \\ h'' \\ h' + f(h) \end{pmatrix}. \tag{4.1}$$

Some trajectories (the same as in figure 2) are represented in figure 5. Notice that the film solution (inset) winds exponentially around a *fixed point* on the h-axis.

4.1.1. *Hydrostatic solutions in the phase space*

For large x, following the reasoning of § 2.5, equation (4.1) becomes linear:

$$\boldsymbol{X}' = \begin{pmatrix} 0 & 1 & 0 \\ 0 & 0 & 1 \\ 0 & 1 & 0 \end{pmatrix} \boldsymbol{X} - \begin{pmatrix} 0 \\ 0 \\ \theta^* \end{pmatrix}. \tag{4.2}$$

Any solution of (4.2) which satisfies the boundary condition (2.7) is included in a plane called E_∞, which may be parameterized by x and the apparent contact angle θ^*_{ap} introduced in § 2.5. E_∞ is defined by the equation $h' + h'' = \theta^*$.

The solutions of the full equation (4.1) which satisfy (2.7) are included in a two-dimensional manifold, called W. This manifold tends to E_∞ for large h. This allows us to approximate numerically the zero-flux film trajectories, for which we impose boundary conditions at $x \to -\infty$ and $x \to +\infty$. We may indeed use a shooting method with initial conditions varying along a constant (large) h line on E_∞. The boundary condition at $x \to +\infty$ is then approximatively satisfied at any step. The shooting method provides an approximation of the only solution that remains constant as x tends to $-\infty$.

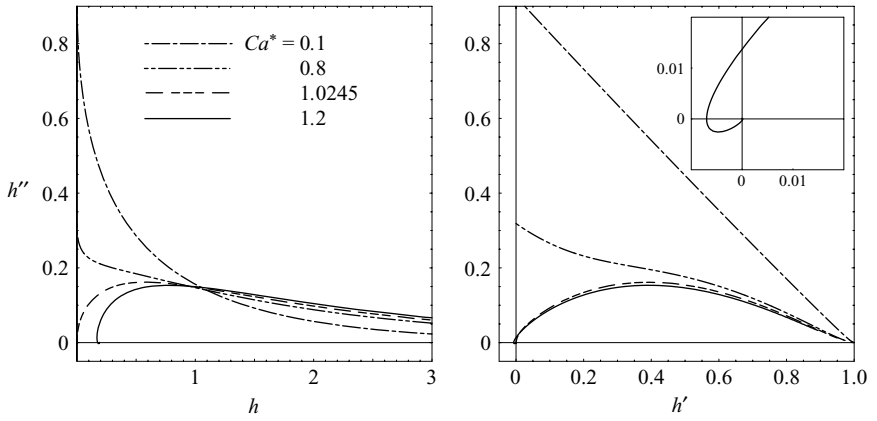

FIGURE 5. Numerical solutions of equation (2.10) for various capillary numbers, represented in phase space (projected on the (h, h'')- and (h', h'')-planes). The rescaled tilt angle θ^* is fixed to 1. The trajectories correspond to the physical solutions shown in figure 2: for sub-critical capillary numbers (the three dashed curves), the trajectory starts at a point on the h''-axis which corresponds to the contact line, whereas, the solid line corresponds to a film solution, and thus does not cross the h''-axis. The inset shows the projection of the film solution on the (h', h'')-plane, at smaller scale.

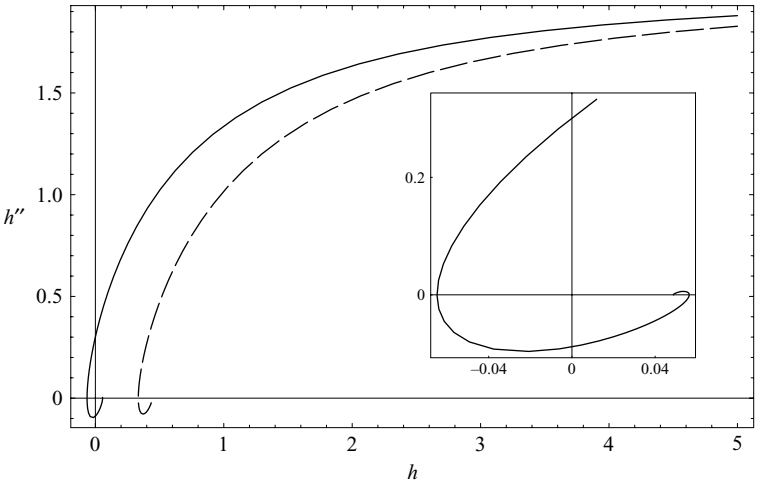

FIGURE 6. Intersection of W (the set of trajectories that tend to a horizontal water surface as x tends to $+\infty$) with the (h, h'')-plane. These curves were obtained by a shooting method with $\theta^* = 2$. Solid line: $Ca^* = 2.1$; dashed line: $Ca^* = 3$. The inset shows the solid curve at a refined scale.

Figure 6 represents the intersection of W with the (h, h'')-plane defined by $h' = 0$, obtained by the shooting method, for two different capillary numbers, above and below Ca_c^*, for $\theta^* = 2$. We observe numerically that the major effect of an increase in Ca^* is a translation in the higher h-direction. The disappearance of the contact-line solution may be described in the following way: any contact-line trajectory is embedded in W, and the boundary conditions impose that it starts on the h''-axis, consequently, it exists if (and only if) there is an intersection between W and the

Condition	Fixed points h_f
$Ca^* < \dfrac{\theta^*}{4}$	None
$Ca^* = \dfrac{\theta^*}{4}$	$-\dfrac{3}{2}$
$Ca^* > \dfrac{\theta^*}{4}$	$\dfrac{3}{2}\left(-1 \pm \dfrac{1}{\sqrt{3}}\sqrt{\dfrac{4Ca^*}{\theta^*} - 1}\right)$

TABLE 1. Existence and values of the fixed points of equation (4.1) (for $Q^* = 0$).

Condition	Eigenvalues
$Ca^* \in \Upsilon(\theta^*)$	a, b, c
$Ca^* \in \partial\Upsilon(\theta^*)$	$a, -a/2, -a/2$
$Ca^* \notin \Upsilon(\theta^*)$	$a, -a/2 + \mathrm{i}\Omega, -a/2 - \mathrm{i}\Omega$

TABLE 2. Eigenvalues of the Jacobian $\boldsymbol{J}_f^+$ at the largest fixed point. a, b, c and Ω are real numbers and

$$\Upsilon(\theta^*) = [(9\theta^{*3}/2)(1 - \sqrt{1 - 1/9\theta^{*2}});\ (9\theta^{*3}/2)(1 + \sqrt{1 - 1/9\theta^{*2}})].$$

When the eigenvalues are real, they satisfy: $a < 0 < b < c$.

h''-axis. Since the main effect of an increase of Ca^* on W is a translation along the h-axis, this intersection disappears above some value Ca_c^* of the capillary number.

4.1.2. *Fixed points*

A fixed point $\boldsymbol{X}_f$ in phase space corresponds physically to a film of constant height h_f:

$$\boldsymbol{X}_f = \begin{pmatrix} 0 \\ 0 \\ h_f \end{pmatrix}.$$

The existence and values of fixed points depend on the parameters θ^* and Ca^*, as presented in table 1. In the following, we will focus on the largest fixed point $\boldsymbol{X}_f^+$, since it is the only one that may be acceptable physically (that is $h_f > 0$). Let us linearize (4.1) around $\boldsymbol{X}_f^+$:

$$\boldsymbol{X}' = \boldsymbol{J}_f^+(\boldsymbol{X} - \boldsymbol{X}_f^+),$$

where $\boldsymbol{J}_f^+$ is the Jacobian of $\boldsymbol{F}$ evaluated at $\boldsymbol{X}_f^+$, that is

$$\boldsymbol{J}_f^+ = \begin{pmatrix} 0 & 1 & 0 \\ 0 & 0 & 1 \\ f'(h_f^+) & 1 & 0 \end{pmatrix}.$$

The local behaviour of solutions around the fixed point depends on the eigenvalues of $\boldsymbol{J}_f^+$, which are presented in table 2. If the eigenvalues are real numbers, one is negative and the two others positive. So there is an unstable manifold of dimension two where the trajectories tend monotonically to the fixed point as x tends to $-\infty$ and a stable manifold S (separatrix) of dimension one. (Note that we stick to the classical definition (we call stable a manifold where trajectories tend to the fixed

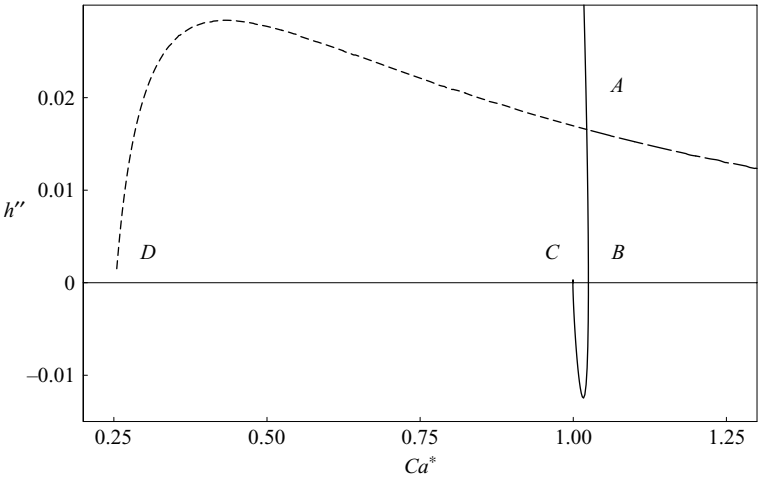

FIGURE 7. Second derivative of the film height against the capillary number, for $\theta^* = 1$. The solid line corresponds to $h''(0)$ for the contact-line solution. The dashed line represents the second derivative of h at the point x_{min} where in the case of a zero-flux film solution, the film is thinnest. Large dashes are used if $h(x_{min}) > 0$, and short dashes otherwise. Points A, B, C and D correspond, respectively, to the following values of Ca^*: $Ca^*_{c,2} \approx 1.0219$, $Ca^*_c \approx 1.0247$, θ^* and $\theta^*/4$. The film corresponding to point A is plotted in figure 4.

point as the variable tends to $+\infty$) even though in that frame only unstable solutions are physically allowed.) On the other hand, when the two eigenvalues are complex conjugate, their common real part is always positive, and the trajectories in the corresponding unstable manifold winds around the fixed point while diverging from it at an exponential rate. In physical space, the fluid surface forms damped stationary waves along the plate (see figure 7). Therefore, the behaviour of W in the vicinity of the fixed point may also be described by this linear expansion. Depending on the parameters, W may either be defined over the whole (h, h')-plane, or tend to the separatrix S (which ends on the fixed point). In the latter case, W winds around the separatrix (as shown in figure 6) or tends to it monotonically. These various regimes are represented in figure 8.

4.1.3. *Critical capillary number*

At any point on the h-axis, $\boldsymbol{X}'$ is parallel to the h''-axis (see equation (4.1)). Consequently, the intersection of W with the (h, h'')-plane (represented on figure 6) has vertical tangent vectors whenever it crosses the h-axis. This explains the behaviour of $h''(0)$ close to the critical capillary number (see figure 3), which may be interpreted as a saddle-node bifurcation. This property is useful for the numerical determination of Ca^*_c at a given θ^*: since we know that the second derivative $h''(0)$ must vanish at the critical capillary number, we may approximate Ca^*_c by a shooting method which varies Ca^* for constant initial conditions (that is, $h(0) = h'(0) = h''(0) = 0$). We show in figure 8 the evolution of the critical capillary number with θ^*, together with the diagram showing the different regimes described above. Notice that since θ^* is a rescaled parameter, we have been able to investigate a large range of values, up to $\theta^* \approx 10^7$.

We did not find any reason for the disappearance of the contact-line solution to coincide with the appearance of the zero-flux film solution as Ca^* is varied. It may well be possible that, as W has already intersected the h''-axis, the zero-flux film trajectory rolls up around the fixed point without h ever becoming negative. Some numerical

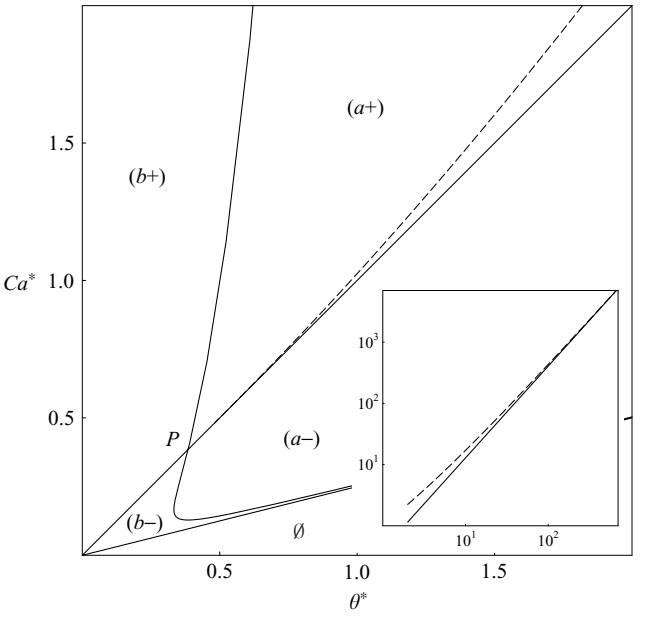

FIGURE 8. Behaviour of W close to the largest fixed point $\boldsymbol{J}_f^+$. $\emptyset$, no fixed point; +, positive fixed point; −, negative fixed point; a, spiralling trajectories; b, monotonic trajectories. Continuous lines delimit the various behaviours. The dashed line represents the critical capillary number above which the contact-line solution disappears Ca_c^*. Inset (logarithmic scale): asymptotic behaviour of the critical capillary number for large θ^* (dashed line) and asymptotic behaviour computed analytically in § 5 (solid line).

simulations give us confidence that hysteresis indeed occurs (that is, $Ca_c^* > Ca_{c,2}^*$): a slight hysteresis may indeed be observed in figure 7. Again, the present study is limited to films of zero flux, and other solutions may exist for the same parameter values. Thus, the hysteresis here observed can only describe a reduced part of the solutions set.

When the capillary number is decreased from a supercritical value, the height of the stationary film h_f decreases, and eventually the film thickness vanishes at some point x_{min} (see figure 7). This point must be a minimum and in that case both $h(x_{min})$ and $h'(x_{min})$ vanish, so this film solution is also a contact-line solution. This explains the change of the sign of $h(x_{min})$ observed at point A in figure 7.

The asymptotic behaviour of Ca_c^* at large θ^* has also been investigated (figure 8). We find that the critical capillary number behaves asymptotically as a power law of the tilt angle, that fits to:

$$Ca_c^* \underset{\theta^* \to \infty}{\sim} 0.3936\,\theta^{*1,4998}. \tag{4.3}$$

This suggest that for high θ^*, Ca_c^* behaves like $\theta^{*3/2}$.

5. Asymptotic results

In the following section, we describe a rough analytical approach, inspired by that of Eggers (2004*a*), which leads to the power law (4.3) for the capillary number obtained numerically in the previous section.

5.1. *Overview*

To determine the dependence of the critical capillary number on the angle, we need to understand better how the solution near the contact line connects with the free surface at infinity. We therefore seek to determine the matching between these two domains. This has actually been done when considering the classical plate-withdrawal problem. It involves a matching between three regions: one near the contact line, a capillary–viscous one and the gravity–capillary interface (Eggers 2004*a*). However, two major differences arise in the present case compared to the usual problem. First, equation (3.1) is regular over the whole range $h \in [0; +\infty[$, whereas in the usual problem, the Navier slip condition (2.3) leads to a pressure divergence at the contact line. However, it has been shown (in the case of an advancing contact line) that the exact form of the slip law near the contact line does not influence the matching procedure with the far-field solution of the free surface (Dussan V. & Davis 1974; Eggers 2004*b*). The second difference lies in the contact angle condition that we consider to be zero instead of small but finite (as for solid plates). Such a condition is crucial as it can be seen from Eggers (2004*a*) where the solutions are expanded in powers of the small parameter Ca/θ_e^3 (θ_e being the static contact angle). Consequently, we cannot obtain a proper matching between the behaviour in the contact-line zone (cubic polynomial at leading order) with the famous logarithmic behavior in the capillary-viscous region:

$$h'(x) = \left[9Ca \ln\left(\frac{\pi}{2^{2/3}\beta^2 x}\right)\right]^{1/3}.$$

However, we can bypass this difficulty by a slight change in the equations leading to a single approximation valid over the first two regions (contact-line zone and capillary–viscous one).

5.2. *A two-zone matching*

The procedure hereinafter presented is based on the assumption that the linear term in the right-hand term denominator of (3.1) is not of fundamental importance. In particular, the coefficient α was arbitrarily set to one at the beginning of this study, but numerical investigations have shown that it may be set to very different values, changing the results by only a few per cent. We therefore set from now on $1/\alpha = 2/\sqrt{3}$ without much change in the equation properties, so that (3.1) reduces to

$$h''' - h' + \theta^* = \frac{Ca^*}{(h/\sqrt{3}+1)^2}. \tag{5.1}$$

Close enough to the contact line, the film slope h' may be neglected owing to the boundary condition (3.1). In addition, close to the critical capillary number, $Ca^* \gg \theta^*$ (this is suggested by the asymptotic behaviour (4.3)), and (5.1) becomes

$$h''' = \frac{Ca^*}{(h/\sqrt{3}+1)^2},$$

which can be solved analytically (as performed by Duffy & Wilson 1997) after the rescaling

$$x = \frac{\sqrt{3}}{(3Ca^*)^{1/3}}\xi, \qquad h(x) = \sqrt{3}(y(\xi) - 1).$$

This rescaling leads to Tanner's problem:

$$y''' = \frac{1}{y^2}, \qquad y(0) = 1, \qquad y'(0) = 0.$$

Its solution may be parameterized in terms of Airy functions Ai and Bi:

$$\xi = 2^{1/3}\frac{\mathrm{Bi}(s_0)\mathrm{Ai}(s) - \mathrm{Bi}(s)\mathrm{Ai}(s_0)}{\mathrm{Bi}'(s_0)\mathrm{Ai}(s) - \mathrm{Bi}(s)\mathrm{Ai}'(s_0)}, \qquad y_{\mathrm{in}} = \frac{1}{\pi^2(\mathrm{Bi}'(s_0)\mathrm{Ai}(s) - \mathrm{Bi}(s)\mathrm{Ai}'(s_0))^2}, \quad (5.2)$$

where s_0 is an integration constant, and s varies between consecutive solutions of equation

$$\mathrm{Bi}'(s_0)\mathrm{Ai}(s) - \mathrm{Bi}(s)\mathrm{Ai}'(s_0) = 0. \quad (5.3)$$

It was shown in § 4.1.3 that, at the critical capillary number, h'' vanishes (and so does y''). This property sets s_0 to zero and the range for s to $[s_1, 0[$, where $s_1 \approx -1.98635$ is the largest solution to (5.3). Matching solution (5.2) with the meniscus solution should provide a condition on Ca^* and θ^*. At large ξ, the behaviour of y_{in} is

$$y_{in} = a\xi^2 + O(\xi)$$

at leading order, where a has the following expression:

$$a = \left(\frac{\mathrm{Bi}'(0)}{2^{1/3}\mathrm{Bi}(s_1)}\right)^2 \approx 0.758947.$$

The second-order Taylor expansion of h_∞ for small x is (see (2.12))

$$h_\infty = A_\infty + \theta^* - \theta^*_{ap} + \theta^*_{ap}x + (\theta^* - \theta^*_{ap})\frac{x^2}{2} + O(x^3).$$

In order to match y_{in} with h_∞, the leading order in the above expression must be x^2, thus

$$\theta^*_{ap} = 0, \qquad A_\infty = -\theta^*.$$

Finally, matching the square terms requires that

$$Ca^*_c \underset{\theta^*\to\infty}{\sim} \frac{1}{(2a)^{3/2}3^{1/4}}\theta^{*3/2}. \quad (5.4)$$

This fits remarkably well with the numerical estimation (4.3), since $1/((2a)^{3/2}3^{1/4}) \approx 0.4063$ (the above numerical fit gives 0.3936). The matching solution is compared to a numerical one in figure 9 for a high value of θ^*, and we observe a remarkable agreement with a reasonably large overlap region. Of course, corrections to this law are expected at next order. In particular, $\theta^*_{ap} = 0$ holds only at the first order of the matching, and it has not been shown here that the apparent contact angle vanishes at the wetting transition.

6. Discussion and conclusions

In this work, a continuum model of the forced dewetting on a porous material has been presented. In the framework of lubrication, an ordinary nonlinear differential equation was derived, close to that investigated by Hocking (2001). Even if the contact angle θ_0 is assumed to vanish, a stationary contact line is found to exist for low dewetting velocity. Moreover, a transition between this steady contact line and the deposit of a liquid film must occur (either an LLD film or free-flux film), since there is a critical capillary number above which no contact-line solution can exist. The transient mechanism of this transition was not studied here.

In the present study, the critical value of the capillary number above which no contact-line solution can be observed behaves asymptotically (for small

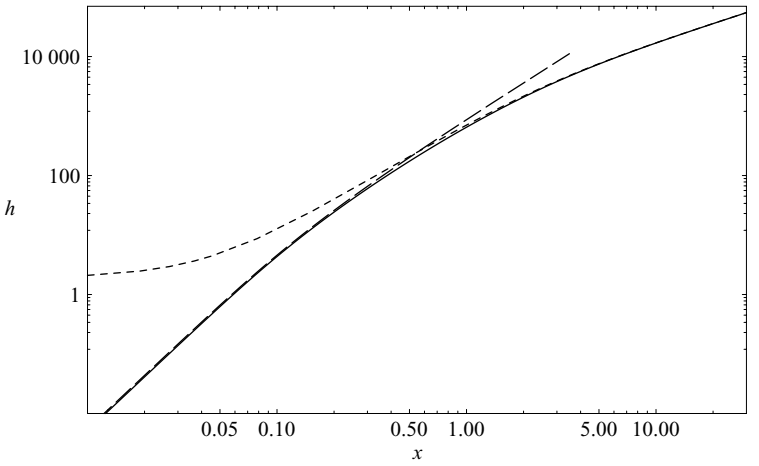

FIGURE 9. Comparison between numerical results (solid line) and the matching presented in this paper in logarithmic scales. $\theta^* \approx 1886$ and $Ca^* \approx Ca_c^* \approx 32870$. Long dashes, analytical solution to Tanner's problem ($\sqrt{3}(1 - y_{in})$); short dashes, capillary–gravity meniscus (y_∞).

non-dimensional slip length λ and small tilt angle θ) as

$$Ca_c \sim \frac{1}{(2a)^{3/2} 3^{1/4}} (\lambda\theta)^{3/2}.$$

The critical capillary number does not vanish even though the contact angle is zero. This comes for the slip condition introduced in § 2, characteristic of porous media. As expected, when the slip length goes to zero, the critical capillary number also vanishes, and the result of Eggers (2004*a*) is recovered.

Another surprising result is the mathematical existence of a family of films that may be deposited on the plate, different from the classical LLD film. Indeed, the thickness of these films is not fixed by the boundary conditions. These *free-flux films* have never been observed experimentally, as far as we know. We have not studied their stability yet, but they will be the subject of further study.

Various conclusions can be drawn from our results regarding the erosion experiment performed by Daerr *et al.* (2003). First, the existence diagram of the contact line can be drawn using the experimental values of the physical parameters. In the present theory, the permeability k of the porous material is crucial, as it is the characteristic slip length at the solid–liquid interface. The value of this parameter may depend strongly on the compaction of the granular material (say between $10^{-12}\,\mathrm{m}^2$ and $900 \times 10^{-12}\,\mathrm{m}^2$, respectively, the value measured by Daerr *et al.* (2003) and the square of the grain size). Figure 10 presents the critical velocities obtained for these two extreme values of the permeability. For the lowest permeability, and down to the smallest withdrawal velocities of the erodible plate, no contact line can exist. On the other hand, when choosing the largest permeability, the critical speed of the contact line is of same order as in the experiment.

The flow acts on the granular medium mainly through the bottom shear rate $\tau = \partial u / \partial Y$, which is known to trigger the erosion process (see Charru, Mouilleron & Eiff 2004). From this shear rate, we can define the Shields number S, which compares

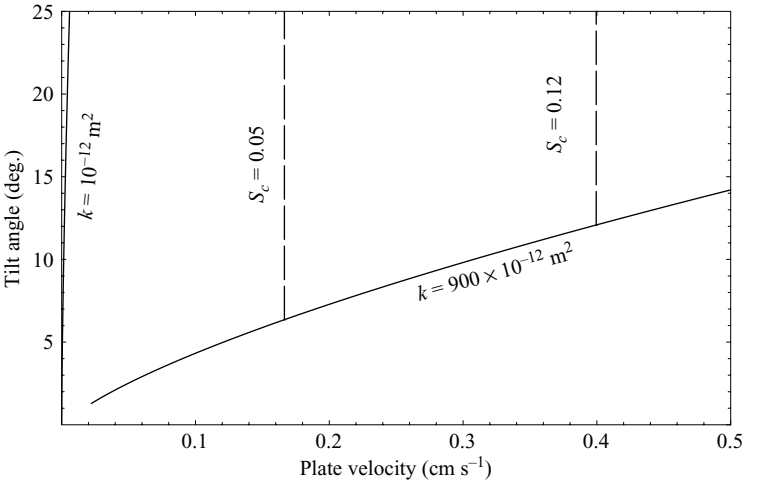

FIGURE 10. Critical speed for two values of the permeability k. For each value of the permeability, a contact line can exist only above the corresponding solid curve. The dashed line represents constant Shields numbers S_c. The values of the physical parameters used in this model are those of Daerr *et al.* (2003): $g = 9.81\,\mathrm{m\,s^{-2}}$, $\rho = 1000\,\mathrm{kg\,m^{-3}}$, $\rho_g = 2750\,\mathrm{kg\,m^{-3}}$, $\eta = 10^{-3}\,\mathrm{kg\,m^{-1}\,s^{-1}}$ and $\gamma_s = 0.07\,\mathrm{N\,m^{-1}}$. The velocity and inclination ranges are those of the experiment.

the viscous force applied to the grains by the flow, to the gravity force:

$$S = \frac{\eta\tau}{(\rho_g - \rho)gd},$$

where ρ_g is the density of the grains (this expression stands only for small tilt angles). Though the erosion process on a granular bed results from discrete and complex phenomena, classical models assume that it starts at a threshold value of the shear rate, at which a critical Shields number S_c is defined (Charru *et al.* 2004). A typical value for S_c is 0.05 (see among others Fredsoe & Deigaard 1992), but Daerr *et al.* (2003) used $S_c = 0.12$ to fit their data. In addition to this large range of possible values, note that the critical Shields number is a function of the slope of the bottom: the more inclined it is, the easier it is for the flow to lift grains, thus the tilt reduces the value of S_c. The shear rate may be deduced from our model, as a function of the dimensionless height of the film h:

$$\tau = \frac{U}{\sqrt{k}} \frac{h - Q^*}{h^2/3 + h + 1}.$$

In the case of a contact line (then $Q^* = 0$), this expression admits a maximum value $\tau_{max} = U/(\sqrt{k}(1 + 2/\sqrt{3}))$ for $h = \sqrt{3}$, that is necessarily reached, since h stretches from zero to infinity. If the Shields number is assumed to be independent of the tilt angle of the plate (to first order), $S = S_c$ defines a vertical line in figure 10 (represented only for $k = 900 \times 10^{-12}\,\mathrm{m^2}$). On the left of such a line, no erosion should occur since the Shields number is smaller than the critical value, thus to account for the erosion patterns observed by Daerr *et al.* (2003) at small velocities, a low value of S_c is required.

Now, if an LLD film covers the plate (then $Q^* > 0$), we are not able to predict analytically the maximum shear rate exerted on the granular bed. However, a sharp

decrease of the shear rate can be expected at the transition from contact line to LLD film, owing to the jump in Q^*. Such a sharp stress variation could provide an explanation for the transition between the different erosion patterns observed by Daerr *et al.* (2003).

At the transition from contact line to LLD film, transient regimes should not be ignored. They have been studied in the literature for non-vanishing contact angles (Hocking 2001), and future studies will aim at understanding the case of zero contact angle, which has been shown here to be quite different.

It is our pleasure to thank Daniel Lhuillier, Pierre-Yves Lagrée, Eric Clément, Florent Malloggi, Peter Spelt and Jens Eggers for stimulating discussions.

Appendix A. Derivation of the fundamental equation

In the following, equation (2.6) is derived from the two-dimensional Navier–Stokes equations. X and Y are dimensional and refer to the axis of figure 1. In the lubrication approximation, and assuming both a permanent regime and small Reynolds number, the momentum conservation reads

$$-\frac{1}{\rho}\frac{\partial p}{\partial X} + g\sin(\theta) + \nu\frac{\partial^2 u}{\partial Y^2} = 0, \tag{A 1a}$$

$$-\frac{1}{\rho}\frac{\partial p}{\partial Y} - g\cos(\theta) = 0, \tag{A 1b}$$

where u and v stand for the water velocity components, respectively, parallel and perpendicular to the plate. Equation (A1 b) may be integrated to give

$$p = \rho g\cos(\theta)(H - Y) + p_L,$$

where p_L is the pressure due to surface tension and H the dimensional water level. Now, if θ is small enough, the slope H' of the free surface should remain reasonably small, so that H'' approximates its curvature, and $p_L \approx -\gamma H''$ (and, similarly, $\sin(\theta) \approx \theta$ and $\cos(\theta) \approx 1$ at first order). The boundary conditions on u at the bottom and the top of the film are (see (2.1), (2.4) and (2.5))

$$u|_{Y=0} + U = \frac{\sqrt{k}}{\alpha}\left.\frac{\partial u}{\partial Y}\right|_{Y=0} - \frac{k}{\eta}\left(\left.\frac{\partial p}{\partial X}\right|_{Y=0} - \rho g\theta\right),$$

$$\left.\frac{\partial u}{\partial Y}\right|_{Y=H(X)} = 0,$$

thus integrating (A 1a) we obtain

$$u = \frac{1}{\nu}\left(\frac{1}{\rho}\frac{\partial p}{\partial X} - g\theta\right)\left(\frac{Y^2}{2} - HY - \frac{\sqrt{k}}{\alpha}H - k\right) + U. \tag{A 2}$$

The water flux withdrawn from the bath through the film is

$$Q = -\int_0^H u\,\mathrm{d}Y.$$

In steady state, mass conservation imposes that Q be a constant, thus

$$\frac{\gamma}{\rho}H''' - gH' + g\theta = \frac{\nu(U - Q/H)}{H^2/3 + H\sqrt{k}/\alpha + k}.$$

If H and X are rescaled by l_c, the nonlinear equation studied throughout this paper is obtained:

$$h''' - h' + \theta = \frac{Ca(1 - Q/(Ul_c h))}{h^2/3 + \lambda h + \lambda^2}.$$

Another rescaling is used from § 2.4: $h = \lambda h^*$. The above equation becomes

$$h'''_* - h'_* + \theta^* = \frac{Ca^*(1 - Q^*/h_*)}{h_*^2/3 + h_* + 1}, \tag{A 3}$$

where $Q^* = Q/(Ul_c\lambda)$ and $\alpha = 1$. In the case of a contact line, no water is removed from the bath and $Q^* = 0$. From § 2.4 to the conclusion, the $_*$ is dropped from h_*.

Appendix B. Pressure divergence at the contact line

We aim here to demonstrate briefly that the classical Navier slip condition, leading to (2.3), is not sufficient to eliminate all the singularities at the contact line, even for a non-vanishing microscopic contact angle ($\theta_e > 0$). Indeed, the dominant order of (2.3) (Eggers 2004*a*; Hocking 1983) near the contact line reads

$$h'''(x) \sim \frac{Ca}{\lambda_N h} \sim \frac{Ca}{\lambda_N \theta_e x},$$

where h and x are dimensionless (by the mean of the capillary length). In the lubrication approximation that we have used throughout, the pressure at the plate then reads

$$p|_{y=0} = \rho g \cos(\theta) l_c h - \frac{\gamma h''}{l_c},$$

and since $h''(x) \sim Ca \ln(x)/\lambda_N\theta_e$, the pressure diverges at the contact line. In the present paper, owing to the permeability of the porous plate, the expansion of h near the contact line is a third-order polynomial ($h \sim h''(0)x^2/2 + (Ca^* - \theta^*)x^3/6$), and thus the pressure does not diverge.

Appendix C. Flow in the porous plate

Using Darcy's law and the conservation of mass, the equation to be solved in the porous plate is

$$\Delta p_p = 0, \tag{C 1}$$

where p_p is the water pressure in the porous medium, with the following boundary conditions:

$$p_p|_{Y=0} = p|_{Y=0},$$
$$\left.\frac{\partial p_p}{\partial Y}\right|_{Y=-e} = \cos(\theta)\rho g.$$

where H, X and Y are the dimensional counterparts of h, x and y. e is the thickness of the plate. Here, the boundary-layer thickness ($\sqrt{k}$) is neglected, this layer being modelled by mean of the slip-law presented in § 2.2.

Assuming that the plate is extremely flat, the term $\partial^2 p_p/\partial X^2$ can be neglected in (C 1) and the pressure field is:

$$p_p = \cos(\theta)\rho g(e - Y) + p|_{Y=0}$$

from which we can deduce the water velocity just under the surface of the porous plate.

Appendix D. Existence of free-flux film solution

Numerical results that show the existence of film solutions to (A 3) for $Q^* = 0$ were presented in § 3. This result seems to be in contradiction with the classical theory of Landau & Levich (1942) where the water flux is fixed by the parameters and boundary conditions. Specifically, Wilson (1982) presents a rigorous asymptotic matching between the film part of the solution (valid for $x \to -\infty$) and the meniscus (at large x), showing that a unique value of the flux allows the matching. On the contrary, we aim to show here that, in addition to the well-known LLD films, there exists another kind of film solution to (A 3), for which the flux is a free parameter in a permanent regime.

(Wilson 1982, p. 212) summarizes the link between boundary conditions and parameters in the following fashion. Equation (A 3) is of third order, so there are three constants to be fixed, in addition to the flux. One these four degrees of freedom corresponds to the origin of x, which can be translated arbitrarily. The water surface becomes flat at large x, so the exponentially growing solution must be ruled out (see § 2.5). The only remaining condition is:

$$\lim_{x \to -\infty} h(x) = h_f,$$

where h_f is the thickness of the deposited film. If λh_f (noted H in Wilson 1982) is small enough, two exponentially growing solutions must be ruled out, the flux is thus fixed. However, as will be shown, this is not the general case, although it is the only one described by Wilson (1982).

Far from the meniscus in the film region, (A 3) links h_f to Q^*:

$$Q^*(h_f) = h_f \left(1 - \frac{\theta^*}{Ca^*} \left(h_f^2/3 + h_f + 1 \right) \right). \tag{D 1}$$

Let us introduce $\delta(x) = h(x) - h_f$ to linearize (A 3) for $\delta \ll h_f$. At first order, we obtain

$$\delta''' - \delta' - \chi \delta = 0, \tag{D 2}$$

$$\chi = \frac{Ca^* \left(Q^*/h_f^2 - \theta^*/Ca^* (2h_f/3 + 1) \right)}{h_f^2/3 + h_f + 1}.$$

It can easily be shown that χ has the same sign as $\mathrm{d}Q^*/\mathrm{d}h_f$. Remembering that any exponential term with a negative growth rate must be ruled out, the following rules can be deduced from (D 2):

(i) if $\chi > 0$, two integration constants are fixed to zero;

(ii) else a single constant is fixed to zero.

In other words, the dimension of the unstable manifold W_u (the set of solutions that tends to $\boldsymbol{X}_f$ for $x \to -\infty$, see § 4) switches from one to two when χ becomes negative. This result is represented in figure 11. In the (h_f, Q^*)-plane, any solution lies on the curve $\mathscr{C}$ defined by (D 1). The LLD film solution is a point on the solid part of the curve, where χ is positive. On the other hand, when χ is negative (dashed line), any point on the curve can be a solution *a priori*. In that case, both the stable manifold W (defined in § 4) and the unstable manifold W_u have dimension two. In the general case, for any Q^*, they intersect on a trajectory that is a film solution. Although we did not strictly prove the existence of such a solution in any case, the numerical solutions presented in figure 11 give us confidence that this result is quite general.

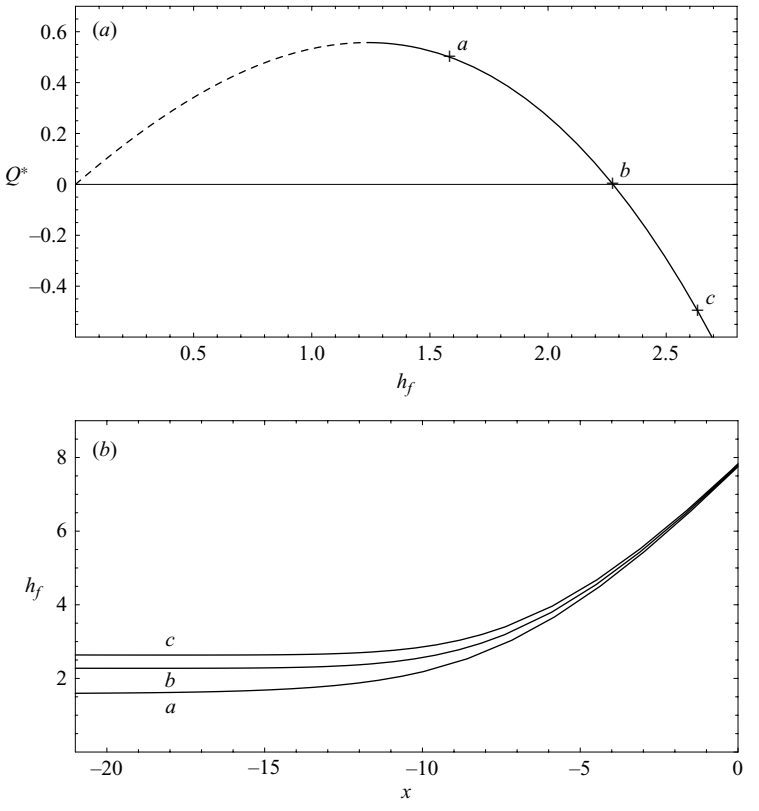

FIGURE 11. (*a*) Non-dimensional water flux withdrawn from the bath (Q^*) as a function of the non-dimensional thickness of the deposited film h_f. The curve is dashed if χ is positive, that is, if the boundary conditions fix Q^*. Any point on the solid part of the curve can represent a full-film solution. The ratio Ca^*/θ^* is fixed to 5 here. (*b*) Three film solutions with different fluxes Q^*. The letters refers to their representation in the (h_f, Q^*)-plane

In addition to the question of the mathematical existence of free-flux film solutions, two physical conditions must be respected if such solutions are to be observed in practice. First, the film thickness has to be positive for any x, which happens at least in some cases, as can be observed on figure 11. Secondly, the solution has to be stable in time: this issue has not been addressed yet.

Finally, it should be noted that the present analysis is very general in the lubrication framework, and does not depend on the specific form of the right-hand side of (A 3). In particular, the result would be similar without any slip-length hypothesis, as long as the contact-line solutions are not considered. These free-flux films will be the subject of future research.

REFERENCES

ARADIAN, A., RAPHAËL, E. & DE GENNES, P.-G. 2000 Dewetting on porous media with aspiration. *Eur. Phys. J.* **2**, 367–376.

BACRI, L. & BROCHARD-WYART, F. 2001 Dewetting on porous media. *Europhys. Lett.* **56**, 414–419.

BEAVERS, S. & JOSEPH, D. 1967 Boundary conditions at a naturally permeable wall. *J. Fluid Mech.* **30**, 197–207.

BLAKE, T. D. & RUSCHAK, K. J. 1979 A maximum speed of wetting. *Nature* **282**, 489–491.

Charru, F., Mouilleron, H. & Eiff, O. 2004 Erosion and deposition of particles on a bed sheared by a viscous flow. *J. Fluid Mech.* **519**, 55–80.

Daerr, A., Lee, P., Lanuza, J. & Clément, E. 2003 Erosion patterns in a sediment layer. *Phys. Rev.* E **67**, 065201.

Derjagin, B. V. 1943 On the thickness of a layer of liquid remaining on the walls of vessels after their emptying, and the theory of the application of photoemulsion after coating on the cine film. *Acta Phys. Chem. USSR* **20**, 349–352.

Duffy, B. R. & Wilson, S. K. 1997 A third-order differential equation arising in thin-film flows and relevent to Tanner's law. *Appl. Math. Lett.* **10** (3), 63–68.

Dussan V., E. B. & Davis, S. H. 1974 On the motion of a fluid–fluid interface along a solid surface. *J. Fluid Mech.* **65**, 71–95.

Eggers, J. 2004*a* Hydrodynamic theory of forced dewetting. *Phys. Rev. Lett.* **93**, 094502.

Eggers, J. 2004*b* Toward a description of contact line motion at higher capillary numbers. *Phys. Fluids* **16**, 3491–3494.

Fredsoe, J. & Deigaard, R. 1992 *Mechanics of Coastal Sediment Transport*. World Scientific.

de Gennes, P., Brochard-Wyart, F. & Quéré, D. 2005 *Gouttes, Bulles, Perles et Ondes*. Belin.

de Gennes, P.-G. 1984 Dynamique d'étalement d'une goutte. *C. R. Acad. Sci. Paris* **298** (4), 111–115.

de Gennes, P.-G. 1985 Wetting: statics and dynamics. *Rev. Mod. Phys.* **57**, 827–863.

Goyeau, B., Lhuillier, D., Gobin, D. & Velarde, M. G. 2003 Momentum transport at a fluid–porous interface. *Intl J. Heat Mass Transfer* **46**, 4071–4081.

Hadjiconstantinou, N. G. 2003 Comment on Cercignani's second-order slip coefficient. *Phys. Fluids* **15**, 2352–2354.

Hervet, H. & de Gennes, P.-G. 1984 Dynamique du mouillage: film précurseur sur solide 'sec'. *C. R. Acad. Sci. Paris* **299**, 499–503.

Hocking, L. M. 1983 The spreading of a thin drop by gravity and capillarity. *Q. J. Mech. Appl. Maths* **36**, 55–69.

Hocking, L. M. 2001 Meniscus draw-up and draining. *Eur. J. Appl. Maths* **12**, 195–208.

Huh, E. & Scriven, L. E. 1971 Hydrodynamic model of steady movement of a solid/liquid/fluid contact line. *J. Colloid Interface Sci.* **35**, 85–101.

Landau, L. D. & Levich, B. V. 1942 Dragging of a liquid by a moving plate. *Acta Phys. Chem. USSR* **17**, 42–54.

Manneville, P. 1990 *Dissipative Structures and Weak Turbulence*. Academic.

Maurer, J., Tabeling, P., Joseph, P. & Willaime, H. 2003 Second-order slip laws in microchannels for helium and nitrogen. *Phys. Fluids* **15**, 2613–2621.

Neale, G. & Nader, W. 1974 Practical significance of Brinkman's extension of Darcy's law – coupled parallel flows within a channel and a bounding porous medium. *Can. J. Chem. Engng* **52**, 475–478.

Raphaël, E. & de Gennes, P.-G. 1999 Imprégnation d'un ruban poreux. *C. R. Acad. Sci. Paris* **327**, 685–689.

Renardy, M., Renardy, Y. & Li, J. 2001 Numerical simulation of moving contact line using a volume-of-fluid method. *J. Comput. Phys.* **171**, 243–263.

Scherer, M. A., Melo, F. & Marder, M. 1999 Sand ripples in an oscillating annular sand-water cell. *Phys. Fluids* **11**, 58–67.

Schorghofer, N., Jensen, B., Kudrolli, A. & Rothman, D. H. 2004 Spontaneous channelization in permeable ground: theory, experiment, and observation. *J. Fluid Mech.* **503**, 357–374.

Seppecher, P. 1996 Moving contact lines in the Cahn–Hilliard theory. *Intl J. Engng Sci.* **34**, 977–992.

Stegner, A. & Wesfreid, J. E. 1999 Dynamical evolution of sand ripples under water. *Phys. Rev.* E **60**, R3487–R3490.

Strogatz, S. H. 1994 *Nonlinear Dynamics and Chaos*. Addison–Wesley.

Wilson, S. D. R. 1982 The drag-out problem in film coating theory. *J. Engng Maths* **16**, 209–221.